Theor Chem Acc (2011) 130:775–788
DOI 10.1007/s00214-011-1028-3

REGULAR ARTICLE

Molecular orbital concept on spin-flip transport in molecular junctions

wave-packet scattering approach and Green's function method

Tomofumi Tada · Takahiro Yamamoto · Satoshi Watanabe

Received: 14 March 2011 / Accepted: 24 August 2011 / Published online: 23 September 2011

Abstract The spin-dependent electron transport correlated with spin-flip dynamics in a molecular junction was investigated in the wave-packet and Green's function approaches. The molecular junction adopted in this work is described by a simple one-dimensional tight-binding chain including a localized spin. The spin exchange coupling J between the localized and conduction electron spins was taken into account through the *s-d* Hamiltonian. The wave-packet simulations showed that the transmission probabilities in both the spin-flip and no-flip processes show large peaks at the eigenvalues of the spin singlet ($-3J/4$) and triplet ($J/4$) states, and that, different transmission properties appear at the mid-gap of the two eigenvalues: the spin-flip process shows a moderate decrease, whereas the no-flip process an abrupt drop. Dividing the *s-d* Hamiltonian into two submatrices and referring to the molecular orbital concept for the coherent electron transport, we found that the moderate decrease in the spin-flip process at the mid-gap is the result of a coherent-and-cooperative contribution from the singlet and triplet states of the conduction and localized electron spins, and that, the abrupt drop in the no-flip process at the mid-gap is mainly caused by the coherent cancellation from the singlet and triplet states. The molecular orbital concept available for the electron transport including spin-flip scattering processes is described in Green's function method, in analogy to the one derived for the spinless electron transport.

Keywords Spin-dependent electron transport · Spin-flip · Molecular junction · Wave packet · Green's function · Molecular orbital

Dedicated to Professor Akira Imamura on the occasion of his 77th birthday and published as part of the Imamura Festschrift Issue.

T. Tada (✉)
Global COE for Mechanical System Innovation (GMSI),
Department of Materials Engineering,
University of Tokyo, Tokyo, Japan
e-mail: tada@cello.t.u-tokyo.ac.jp

T. Yamamoto
Department of Liberal Arts, Faculty of Engineering,
Tokyo University of Science, Tokyo, Japan
e-mail: takahiro@rs.tus.ac.jp

S. Watanabe
Department of Materials Engineering, University of Tokyo,
Tokyo, Japan
e-mail: watanabe@cello.t.u-tokyo.ac.jp

1 Introduction

Localized spins in bulk materials, on substrates, and in single molecules have been identified as attractive candidates for nanoscale devices and information technology [1–13] and have been detected using inelastic spin-flip measurements [14–24]. When the localized spin is captured in/on a metallic substrate or sandwiched between electrodes, the system can be regarded as a metallic system including a magnetic impurity as a localized spin. In the magnetic impurity systems, the Kondo effect is a key many-body effect for the spin-dependent electron transport in which the direction of the localized spin is highly correlated with the spin-flip processes of many electrons in the metal. The spin-dependent scattering states, however, include multiple spin-flip processes, and thus, the identification of the spin states from the measured current is a hard task. In addition to this, the moderate couplings of a single molecule with substrate or metallic nanowires make the electron transport properties sensitive to the contact structures [25–32], resulting in the difficulty on the control of

the electron transport through a single molecule. However, the high self-assembling property of molecules on the substrate is a quite attractive feature for the fabrication of well-defined nanoscale device structures. Thus, the understanding and control of spin-flip dynamics in molecular junctions will extend the possibility of a single spin on a molecule in the field of nanoelectronics.

The wave-packet propagation is one of the powerful theoretical tools for systems including *complicated* interactions such as electron–phonon interactions because the time propagation of the wave-packet can be carried out in a straightforward manner using the system Hamiltonian. The wave-packet propagations, thus, have been applied to various issues (e.g., inelastic electron transport including electron–phonon couplings [33], ballistic-to-diffusive electron transport [34], charged carrier migration in organic systems [35], and phonon transport in nanostructures [36]). The wave-packet approaches have been adopted also for spin systems in a Hubbard model [37], but the details of the spin-flip processes in nanostructures are not so clear, especially for what can be represented in the wave-packet dynamics. For example, the applicability of the wave-packet dynamics including the spin-flip for the Kondo effect [15, 17–21] in molecular spin systems is quite unclear, although the advanced theoretical tools based on many-body Green's function are applicable for the Kondo effect [38].[1]

In this study, we carried out wave-packet simulations and Green's function calculations to investigate spin-dependent electron transport in molecular junctions modeled by a simple one-dimensional tight-binding chain including the spin exchange coupling between conduction and localized electron spins. We firstly simulate the electron spin conduction including spin-flip processes based on the wave-packet approach and analyze the spin-flip processes caused by the spin exchange coupling. In this study, we use the term *spin-flip transport* to express the spin-dependent electron transport correlated with the spin-flip dynamics on a single molecule. Based on the simulated spin-flip transport, we characterize the spin-dependent transmission probabilities in a spin subspace constituted by a direct product of conduction and localized electron spins. In the characterization, we first found that the spin-flip transport is classified into the two cases, flip and no-flip processes, and second found that the classification in turn enables us to represent the spin-flip transport in Green's function method in the coherent regime in which spin-flip transport is successfully characterized with a molecular orbital concept. The orbital concept for the spin-flip transport corresponds to a simple extension to the one derived in spinless cases proposed by one of the authors [39]. Finally we have figured out how the incoherent spin-flip processes that are automatically included in the wave-packet dynamics are represented in the Green's function approach in order to determine what is and more importantly what is not included in the wave-packet simulations.

[1] The accuracy of the calculations based on the many-body Green's function depends on how the electron-electron interaction is reasonably truncated in self-energy through the Feynman diagrams. It requires technical skills and experience with Feynman diagrams. On the other hand, in the wave-packet simulations, the wave-packet propagates without any approximations, which is much simpler than in the many-body Green's function, although whether the wave-packet simulation using the *s-d* Hamiltonian is applicable for the many-body effect is unclear.

2 Wave-packet scattering dynamics for the spin-flip transport

The one-dimensional tight-binding model adopted in the spin-flip simulation is shown in Fig. 1. The Hamiltonian of this system can be represented in the *s-d* model [40] (see also Appendix 1), and the matrix elements are shown as

$$\mathbf{H} = \begin{pmatrix} \mathbf{H_L} & \mathbf{t_L^\dagger} & \mathbf{0} \\ \mathbf{t_L} & \mathbf{H_s} & \mathbf{t_R^\dagger} \\ \mathbf{0} & \mathbf{t_R} & \mathbf{H_R} \end{pmatrix}, \tag{1}$$

where

$$\mathbf{H_L} = \begin{array}{c} \\ \vdots \\ s-4_\downarrow \\ s-3_\uparrow \\ s-3_\downarrow \\ s-2_\uparrow \end{array} \begin{array}{c} \cdots \quad s-4_\downarrow \quad s-3_\uparrow \quad s-3_\downarrow \quad s-2_\uparrow \\ \begin{pmatrix} \ddots & \ddots & \ddots & \ddots & \\ \ddots & \varepsilon_0 & 0 & -t & 0 \\ \ddots & 0 & \varepsilon_0 & 0 & -t \\ \ddots & -t & 0 & \varepsilon_0 & 0 \\ & 0 & -t & 0 & \varepsilon_0 \end{pmatrix} \end{array}, \tag{2}$$

$$\mathbf{H_s} = \begin{array}{c} \\ s-2_\downarrow \\ s-1_\uparrow \\ s-1_\downarrow \\ s_{\uparrow\Downarrow} \\ s_{\downarrow\Uparrow} \\ s+1_\uparrow \\ s+1_\downarrow \\ s+2_\uparrow \end{array} \begin{array}{c} s-2_\downarrow \quad s-1_\uparrow \quad s-1_\downarrow \quad s_{\uparrow\Downarrow} \quad s_{\downarrow\Uparrow} \quad s+1_\uparrow \quad s+1_\downarrow \quad s+2_\uparrow \\ \begin{pmatrix} \varepsilon_0 & 0 & -t & & & & & \\ 0 & \varepsilon_0 & 0 & -t' & & & & \\ -t & 0 & \varepsilon_0 & 0 & -t' & & & \\ & -t' & 0 & \frac{-J}{4} & \frac{J}{2} & -t' & & \\ & & -t' & \frac{J}{2} & \frac{-J}{4} & 0 & -t' & \\ & & & -t' & 0 & \varepsilon_0 & 0 & -t \\ & & & & -t' & 0 & \varepsilon_0 & 0 \\ & & & & & -t & 0 & \varepsilon_0 \end{pmatrix} \end{array}, \tag{3}$$

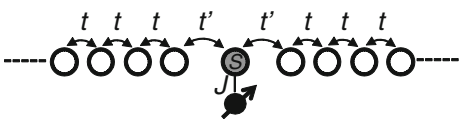

Fig. 1 Tight-binding one-dimensional model including a localized electron spin. The *gray atom* (or molecule) is coupled to a localized spin (*black*) through the spin exchange coupling *J*, and is sandwiched between the one-dimensional electrodes (*white*). The nearest neighbor hopping integrals are represented by *t* and *t'*

$$\mathbf{H_R} = \begin{array}{c} \\ s+2_\downarrow \\ s+3_\uparrow \\ s+3_\downarrow \\ s+4_\uparrow \\ \vdots \end{array} \begin{array}{c} \begin{array}{ccccc} s+2_\downarrow & s+3_\uparrow & s+3_\downarrow & s+4_\uparrow & \cdots \end{array} \\ \begin{pmatrix} \varepsilon_0 & 0 & -t & 0 & \\ 0 & \varepsilon_0 & 0 & -t & \ddots \\ -t & 0 & \varepsilon_0 & 0 & \ddots \\ 0 & -t & 0 & \varepsilon_0 & \ddots \\ & \ddots & \ddots & \ddots & \ddots \end{pmatrix} \end{array}, \tag{4}$$

$$\mathbf{t_L} = \begin{array}{c} \\ s-2_\downarrow \\ s-1_\uparrow \\ s-1_\downarrow \\ \vdots \end{array} \begin{array}{c} \begin{array}{ccccc} \cdots & s-3_\uparrow & s-3_\downarrow & s-2_\uparrow \end{array} \\ \begin{pmatrix} \cdots & 0 & -t & 0 \\ & & 0 & -t \\ & & & 0 \\ & & & \vdots \end{pmatrix} \end{array}, \tag{5}$$

and

$$\mathbf{t_R} = \begin{array}{c} \\ s+2_\downarrow \\ s+3_\uparrow \\ s+3_\downarrow \\ \vdots \end{array} \begin{array}{c} \begin{array}{ccccc} \cdots & s+1_\uparrow & s+1_\downarrow & s+2_\uparrow \end{array} \\ \begin{pmatrix} \cdots & 0 & -t & 0 \\ & & 0 & -t \\ & & & 0 \\ & & & \vdots \end{pmatrix} \end{array}. \tag{6}$$

In these matrix elements,[2] s is the site number of the sandwiched atom (atom S) coupled to the localized spin. The symbols, $\uparrow$ and $\downarrow$, correspond to the spin directions of electrons, and $\Uparrow$ and $\Downarrow$ are those of the localized spin. In this study, we focused our attention on the anti-ferromagnetic coupling between the conduction and localized electron spins $\uparrow\Downarrow$ and $\downarrow\Uparrow$, because the ferromagnetic elements $\uparrow\Uparrow$ and $\downarrow\Downarrow$ do not lead to the spin-flip processes (see Appendix 1). The on-site energy ε_0 and hopping integral in electrodes t are, respectively, set to be 0 and 1 in this study. Using the Hamiltonian matrix, we can propagate wave packets in the Crank-Nicholson scheme [41], in which the norm of the wave packet is completely conserved (see Appendix 2).

$$\psi(x_i, t+\Delta t) = \frac{1+\frac{1}{i\hbar}\frac{\Delta t}{2}H}{1-\frac{1}{i\hbar}\frac{\Delta t}{2}H}\psi(x_i, t). \tag{7}$$

The index x_i is the position of the i-th site, and Δt is the time step in the wave-packet propagation. In a practical way for solving the equation, we adopted an alternative form of Eq. 7 as

$$\psi(x_i, t+\Delta t) = \chi - \psi(x_i, t), \tag{8}$$

where χ is calculated from the following equation, in which a function Q is defined as $Q = \frac{1}{2}\left(1 + i\frac{\Delta t}{2\hbar}H\right)$,

$$Q\chi = \psi(x_i, t). \tag{9}$$

Since the Hamiltonian matrix in the present model is a band matrix, the linear equation for the propagation of wave packets is convenient with respect to the computational time and memory saving.

The number of the sites in the whole system is 10,000 in total, and thereby the size of the Hamiltonian matrix $\mathbf{H}$ is 20,000 × 20,000. The spin site s is equal to the mid-position of the system, 10,000. As for the initial wave packet, we constructed the spin-up Gaussian wave-packets from the eigenvectors of the one-dimensional electrode [42].[3] To prepare wave-packets having a sufficiently fine energy resolution, Gaussian wave-packets with the broadening width of about 1,200 sites were adopted in this study (see Appendix 3 for the details of the computational conditions and the units used in this study).

Figure 2 shows a typical dynamics of the wave-packet with the energy of the Fermi level of the one-dimensional electrode. The initial packet at 0 fs is perfectly polarized to the up-spin, and its velocity is oriented to the right direction. When the wave-packet reaches the site of atom S, a portion of the wave-packet is reflected or transmitted by the hopping integral t', accompanied by the spin-flip processes caused by the spin exchange coupling J. Counting the amplitudes of transmitted wave-packet in the right electrode, we can calculate transmission probabilities in terms of spin-flip processes (i.e., up-to-up ($\uparrow - \uparrow$) and up-to-down ($\uparrow - \downarrow$)) as

$$T_{\uparrow-\uparrow}(E) = \frac{\sum_{i\in R}|\psi^E_\uparrow(x_i, t_1)|^2}{\sum_{i\in L}|\psi^E_\uparrow(x_i, t_0)|^2}, \tag{10}$$

and

$$T_{\uparrow-\downarrow}(E) = \frac{\sum_{i\in R}|\psi^E_\downarrow(x_i, t_1)|^2}{\sum_{i\in L}|\psi^E_\uparrow(x_i, t_0)|^2}, \tag{11}$$

where L/R is the left/right electrodes, and E is the energy of the propagating wave-packet. t_0 is the initial time, and t_1 is an arbitrary time after the spin-flip transmission/reflection

[2] The matrix of the left (right) hand side electrode H_L (H_R) is written as a semi-infinite matrix in Eqs. 2 and 4. When the wave-packet simulation is carried out, the matrix size must be finite to obtain the propagation matrix, but in Green's function method the matrix size is correctly semi-infinite, which is taken into account through the surface Green's function technique. The finiteness of the matrices in the wave-packet simulation sometimes causes artificial errors in the calculations of transmission functions, but we simply avoid the problem by using a large matrix. The details are described in Appendix 3.

[3] The wave-packet amplitudes calculated in a spin unpolarized one-dimensional tight-binding chain were assigned to those only for up-spin sites in the left-electrode of the *s-d* model. This corresponds to the initial condition for the antiferromagnetic coupling between the incoming electron spin and localized spin.

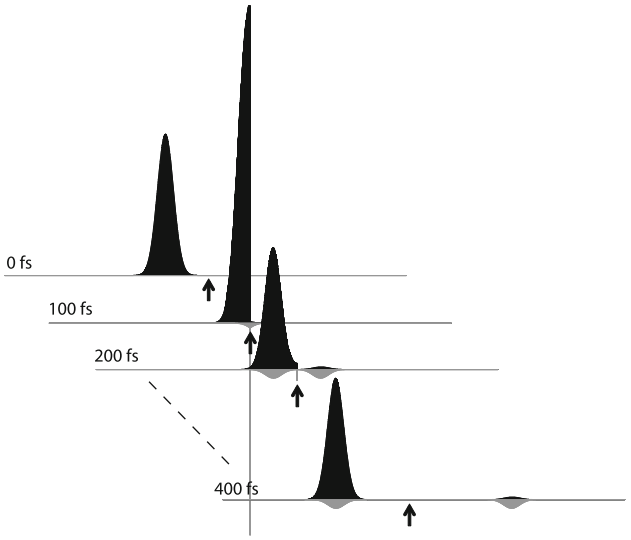

Fig. 2 Wave-packet propagations using the tight-binding parameters of $t' = 0.1t$ and $J = 0.2t$. The *black arrow* is the site of the sandwiched atom (or molecule) coupled to the localized spin. The time step is set to be 0.5 fs. (The time scale in the wave-packet propagation is calculated by assuming that the transfer integral is 2.7 eV and the distance between the nearest neighbors is 1.4 Å, which are the typical parameters for carbon. See Appendix 3 for the details.) The *squared amplitudes* of wave-packet $|\psi|^2$ above/below the *horizontal axis* correspond to those of conduction electrons with up/down-spin

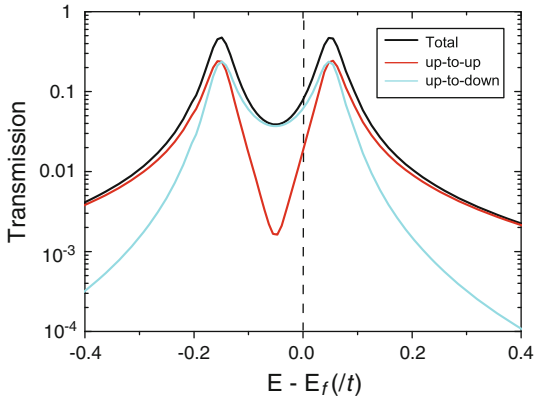

Fig. 3 Calculated transmission probabilities for the up-to-up and up-to-down processes. The total transmission is the sum of the two processes. The tight-binding parameters are $t' = 0.1t$ and $J = 0.2t$

(e.g., 400 fs in Fig. 2). Executing the time propagation of the wave-packet within any energy window $\{E\}$, we obtain the process-dependent transmission probabilities as a function of energy.

Figure 3 shows the calculated transmission probabilities, $T_{\uparrow\to\uparrow}(E)$ and $T_{\uparrow\to\downarrow}(E)$. Both processes show the two peaks at the energies of $-0.15\ t$ and $0.05\ t$. Since the 2×2 matrix for atom S in the basis of $s_{\uparrow\Downarrow}$ and $s_{\downarrow\Uparrow}$ in Eq. 3 has $-J/4$ for the diagonal elements and $J/2$ for the off-diagonal elements, the eigenvalues of the singlet and triplet states are $-3J/4$ and $J/4$, respectively. The spin exchange coupling J is $0.2\ t$ in this calculation, and thus, the two peaks in T correspond to the electron transmission through the singlet and triplet states of the conduction and localized electron spins. On the other hand, at the mid-gap between the two eigenlevels (i.e., $-J/4$), the transmission probabilities show different properties depending on the spin-flip processes: $T_{\uparrow\to\uparrow}$ shows an abrupt drop, but $T_{\uparrow\to\downarrow}$ a moderate drop at the energy. Since the wave-packet dynamics in the present Hamiltonian includes multiple spin-flip scattering processes at the spin site as ↑-to-↑, ↑-to-↓, ↑-to-↓-to-↑, and so on, a simple analysis of the time propagation of the wave-packets is not so successful for the understanding of the precise picture in the spin-flip processes. It is to be noted that if the lifetime of the conduction electron at the site of atom S significantly depends on the flip cycle, we may obtain a transmitted wave-packet showing multiple peaks, and we may successfully divide the transmitted wave-packet in terms of the flip cycle. However, such a situation can appear only for a limited condition depending on the ratio of J and t', and thus, the direct division of the transmitted wave-packet is not a successful way for general cases. In fact, we did not observe such multiple peaks in the transmitted wave-packet within the parameter ranges of $0.01\ t \leq J \leq 0.5\ t$ and $0.01\ t \leq t' \leq 0.5\ t$.

In the present section, we demonstrated the wave-packet simulations in which the time propagation is governed by the Hamiltonian. The wave-packet dynamics, therefore, automatically include coherent and incoherent scattering processes when the system Hamiltonian includes an interaction leading to such processes. However, one of the important points to be investigated more precisely is to understand what is represented in the wave-packet propagations.

3 Green's function approach for electron transport

To analyze the *spin-flip transport* in a well-defined model, we introduce Green's function approach in this section. As we will explain in the later part of this section, we found that a molecular orbital (MO) concept in electron transport is useful also for the spin-flip transport. Let us briefly explain the molecular orbital concept in electron transport without spin-flips before the analysis of the spin-flip transport.

3.1 Molecular orbital concept for electron transport without spin-flips

Here, we introduce a two-site model (molecule) connected to one-dimensional electrodes, which mimics molecular junctions. Figure 4 shows the two important contact structures in the understanding of the MO concept in

electron transport: both sites in the molecule are connected to electrodes as shown in Fig. 4a, and only one site is connected to the electrodes in Fig. 4b. The matrix elements in the tight-binding model for these systems are shown as

$$\mathbf{H_A} = \begin{array}{c} \\ \vdots \\ \alpha_1 \\ \alpha_2 \\ \vdots \end{array} \begin{array}{c} \cdots \quad\quad\quad\quad \alpha_1 \quad \alpha_2 \quad\quad\quad\quad \cdots \\ \begin{pmatrix} \ddots & \ddots & & & & & & & \\ \ddots & \varepsilon_0 & -t & & & & & & \\ & -t & \varepsilon_0 & -t' & & & & & \\ & & -t' & \varepsilon_\alpha & -t'' & & & & \\ & & & -t'' & \varepsilon_\alpha & -t' & & & \\ & & & & -t' & \varepsilon_0 & -t & & \\ & & & & & -t & \varepsilon_0 & \ddots & \\ & & & & & & \ddots & \ddots & \end{pmatrix} \end{array}, \tag{12}$$

and

$$\mathbf{H_B} = \begin{array}{c} \\ \vdots \\ \alpha_1 \\ \alpha_2 \\ \vdots \end{array} \begin{array}{c} \cdots \quad\quad\quad\quad \alpha_1 \quad \alpha_2 \quad\quad\quad\quad \cdots \\ \begin{pmatrix} \ddots & \ddots & & & & & & & \\ \ddots & \varepsilon_0 & -t & & & & & & \\ & -t & \varepsilon_0 & -t' & & & & & \\ & & -t' & \varepsilon_\alpha & -t'' & -t' & & & \\ & & & -t'' & \varepsilon_\alpha & 0 & & & \\ & & & -t' & 0 & \varepsilon_0 & -t & & \\ & & & & & -t & \varepsilon_0 & \ddots & \\ & & & & & & \ddots & \ddots & \end{pmatrix} \end{array}, \tag{13}$$

for the contact structures in Fig. 4(a) and (b), respectively. ε_0 and ε_α are, respectively, the on-site energies of atoms in the electrodes and in molecule. In the later part of this section, we will come back to these matrix expressions to point out the similarity of those between the above and the spin-flip cases.

In Green's function approach for electron transport, the transmission probability T is expressed in terms of the advanced/retarded Green's functions $\mathbf{G}^{A/R}$ of molecule and the local density of states ρ of the apex atom in each electrode as follows [43].

$$T_{rs}(E) = \frac{(2\pi t'^2)^2}{2} G^A_{sr}(E) G^R_{rs}(E) \rho(E) \rho(E). \tag{14}$$

In this expression, we use the fact that the molecule is connected to each electrode through a single hopping parameter t'. The $G^{A/R}_{sr}(E)$ is a matrix element of the advanced/retarded Green's function $\mathbf{G}^{A/R}(E)$, which is represented as $\mathbf{G}^{A/R}(E) = \left[E\mathbf{1} - \mathbf{H}_{mol} - \mathbf{\Sigma}^{A/R}_L - \mathbf{\Sigma}^{A/R}_R\right]^{-1}$, where $\mathbf{H}_{mol}$ is the 2×2 Hamiltonian matrix in the basis of α_1, α_2 in the two site models, and $\mathbf{\Sigma}_{L/R}$ is the 2×2 self-energy matrix of the left/right electrodes. Since the interaction between the molecule and each electrode is represented by a single hopping t', the self-energy matrix has a single non-zero element (e.g., $(\mathbf{\Sigma}_L)_{i,j} = t'^2 g_{\mathrm{elec}} \delta_{ij} \delta_{i1}$ and $(\mathbf{\Sigma}_R)_{i,j} = t'^2 g_{\mathrm{elec}} \delta_{ij} \delta_{i2}$ for Contact A, where g_{elec} is Green's function of the electrodes). In the matrix representation of Green's function method for electron transport, the transmission probability is calculated as $T(E) = \mathrm{Tr}[i\{\mathbf{\Sigma}^R_L(E) - \mathbf{\Sigma}^A_L(E)\}\mathbf{G}^R(E) i\{\mathbf{\Sigma}^R_R(E) - \mathbf{\Sigma}^A_R(E)\}\mathbf{G}^A(E)]$ [44], and by bearing what we mentioned about the matrix elements, the expression of $T(E)$ shown in Eq. 14 can be obtained. The indices r, s in Eq. 14, thereby, correspond to the sites in the molecule connected to the electrodes, that is, the indices r, s are, respectively, equal to α_1, α_2 in Contact A and α_1, α_1 in Contact B.

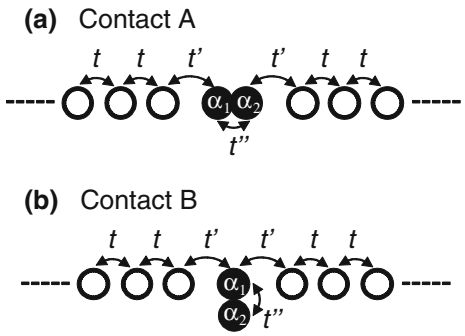

Fig. 4 One-dimensional tight-binding molecular junctions for the two site model. The *black symbols* are the two atoms, α_1 and α_2, of the sandwiched molecule. We adopted the nearest-neighbor hoppings in the electrode, t, at the contact with the molecule, t', and in the molecule, t''. **a** Contact A: both atoms in the molecule are attached to the electrodes. **b** Contact B: a single atom in the molecule is attached to the electrodes

Figure 5 shows the calculated transmission probabilities for Contact A and Contact B. In both cases, the transmission probabilities show the sharp peaks at the energy of $-1.0\ t$ and $1.0\ t$, because the eigenvalues of the highest occupied MO (HOMO) and lowest unoccupied MO (LUMO) of the sandwiched molecule are $-1.0\ t$ and $1.0\ t$, respectively. It is to be noted that the tight-binding parameters for the molecule adopted in the calculation are $t'' = t$ and $\varepsilon_\alpha = \varepsilon_0 = 0$. At the mid-gap between the HOMO and LUMO, on the other hand, the two contacts show different properties in the transmission probabilities: the transmission for Contact B drops to zero, whereas Contact A shows a moderate decrease. To understand these transmission properties, the analysis of Green's function $G_{sr}(E)$ is quite useful. According to the pioneering study for electron tunneling by Caroli and co-workers [43], Green's function $G_{sr}(E)$ is given in terms of the unperturbed Green's function $G^{A/R}_{sr}(E)$ as

$$G_{rs} = \frac{G^{(0)}_{rs}}{D}, \tag{15}$$

where

$$D = (1 - t'^2 G_{ss}^{(0)} g_{\mathrm{elec}})(1 - t'^2 G_{rr}^{(0)} g_{\mathrm{elec}}) - t'^4 G_{rs}^{(0)} G_{sr}^{(0)} g_{\mathrm{elec}} g_{\mathrm{elec}}. \quad (16)$$

Here, we dropped the notation of "retarded/advance" and the energy E for the simplicity. When the electrode–molecule interaction is weak (i.e., small hopping t'), the function D can be approximated to 1. Thus, in weak interaction cases, we can analyze the unperturbed Green's function $G^{(0)}$ instead of the perturbed Green's function G to figure out the properties involved in Green's function.

The unperturbed Green's function of the molecule can be written in terms of molecular orbitals as

$$G_{rs}^{(0)}(E) = \sum_k \frac{C_{rk} C_{sk}}{E - \varepsilon_k}. \quad (17)$$

The k-th eigenvalue of the isolated molecule is ε_k, and its eigenvector (i.e., orbital coefficient) on the site r is C_{rk}. Here, we used the fact that the coefficients $C's$ of the molecule are real numbers. At the mid-gap between HOMO and LUMO of the molecule, the two contributions from HOMO and LUMO are clearly significant terms in $G^{(0)}$. It is to be noted that this situation is exactly true in the present two-site model, because we just have the two MOs only, HOMO and LUMO.

Since the energy differences $E - \varepsilon_k$ appear in the denominator and the orbital coefficients in the numerator in $G^{(0)}$, we can readily derive the following orbital relation in electron transport [39]: (i) large orbital coefficients at the contact sites, C_{rk} and C_{sk} for k = HOMO or LUMO, lead to a large transmission probability, and (ii) the opposite sign between the two terms, $C_{r\,\mathrm{HOMO}}\, C_{s\,\mathrm{HOMO}}$ and $C_{r\,\mathrm{LUMO}}\, C_{s\,\mathrm{LUMO}}$, is required for a cooperative contribution from HOMO and LUMO in the transmission probability at the mid-gap, because of the denominator $E - \varepsilon_k$ in $G^{(0)}$. In other words, when the two terms show the same sign, the contributions from HOMO and LUMO are canceled out at the mid-gap.

Let us consider the transmission probability of the two-site model with respect to the orbital rules. The orbital phases of HOMO and LUMO of the two-site molecule are shown in Fig. 6. In this model, the amplitude of the orbital coefficients is $1/\sqrt{2}$, regardless of the site and eigenlevel. Thus, the orbital rule we have to take care is rule (ii) in the present model. In Contact A, the sites connected to the electrodes are α_1 and α_2. The numerator in $G^{(0)}$ for HOMO, $C_{\alpha\_1\mathrm{HOMO}}\, C_{\alpha\_2\mathrm{HOMO}}$, is a positive number, but for LUMO, $C_{\alpha\_1\mathrm{LUMO}}\, C_{\alpha\_2\mathrm{LUMO}}$ is a negative number. This is the case of the cooperative contribution for the electron transmission at the Fermi level, leading to the moderate decrease in transmission at the Fermi level as shown in Fig. 5. In Contact B, on the other hand, the site connected to the electrodes is α_1 only, and the terms $C_{\alpha\_1\mathrm{HOMO}}\, C_{\alpha\_1\mathrm{HOMO}}$ and $C_{\alpha\_1\mathrm{LUMO}}\, C_{\alpha\_1\mathrm{LUMO}}$ have the same sign (i.e., positive) and the same value. Thereby the unperturbed Green's function $G^{(0)}$ at the Fermi level is exactly zero, resulting in the sharp drop of transmission probability at the Fermi level, as shown in Fig. 5. This is the molecular orbital concept available for the understanding of electron transport in spinless systems. The applications of the orbital rules for electron transport in more complicated molecules can be found elsewhere [39, 45–52].

3.2 Orbital concept for the spin-flip transport

The orbital concept introduced in the previous part is also useful for spin polarized cases if there are no spin-flip processes, because we can write down the matrix elements for each spin independently. However, when spin-flip processes are allowed by the spin exchange coupling, the matrix elements are not divided into submatrices in terms of up- or down-spins any more. For example, such a division of the whole matrix in Eq. 1 will fail, because of the off-diagonal element in the basis of $s_{\uparrow\Downarrow}$ and $s_{\downarrow\Uparrow}$. However, focusing our attention on the spin directions of transmitted electrons in the right electrode (i.e., the drain electrode), we found that the division of the whole matrix in terms of the spin-flip processes is convenient in the

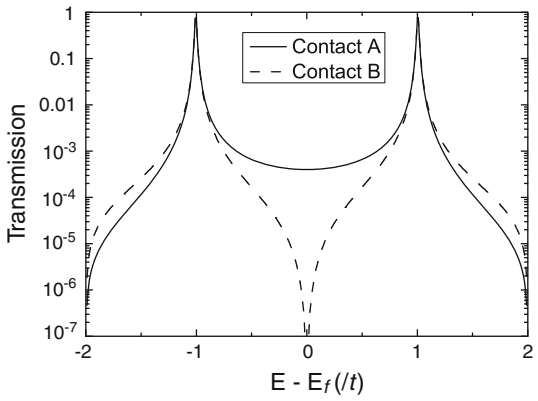

Fig. 5 Calculated transmission probabilities for the two contact cases, Contact A and Contact B. The tight-binding parameters used in this calculations are $t' = 0.1\ t$, $t'' = t$, and $\varepsilon_\alpha = \varepsilon_0 = 0$

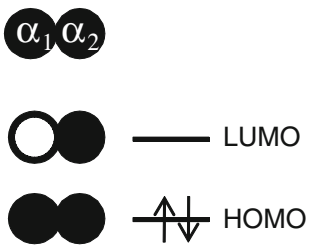

Fig. 6 Orbital phases of HOMO and LUMO of the two site molecule. The *black symbol* means a positive coefficient, and the *white negative*

understanding of the spin-flip transport: (i) ↑-to-↑ without the spin-flip for the transmitted electron spin and (ii) ↑-to-↓ through the spin-flip for the transmitted electron spin. It is worth mentioning that there are many possibilities for the division pattern of the whole matrix (e.g., ↑-to-↓-to-↑ is also possible), but we found the two divisions are useful for the understanding of the spin-flip transport as described in this section.

The whole matrix in Eq. 1 is thus divided into the following submatrices.[4]

$$\mathbf{H}^{(1)}_{s\uparrow-\downarrow} = \begin{array}{c} \\ \vdots \\ s-2_\uparrow \\ s-1_\uparrow \\ s_{\uparrow\Downarrow} \\ s_{\downarrow\Uparrow} \\ s{+}1_\downarrow \\ s{+}2_\downarrow \\ \vdots \end{array} \begin{array}{c} \cdots \quad s-2_\uparrow \quad s-1_\uparrow \quad s_{\uparrow\Downarrow} \quad s_{\downarrow\Uparrow} \quad s{+}1_\downarrow \quad s{+}2_\downarrow \quad \cdots \\ \begin{pmatrix} \ddots & \ddots & & & & & & \\ \ddots & \varepsilon_0 & -t & & & & & \\ & -t & \varepsilon_0 & -t' & & & & \\ & & -t' & \frac{-J}{4} & \frac{J}{2} & & & \\ & & & \frac{J}{2} & \frac{-J}{4} & -t' & & \\ & & & & -t' & \varepsilon_0 & -t & \\ & & & & & -t & \varepsilon_0 & \ddots \\ & & & & & & \ddots & \ddots \end{pmatrix} \end{array}, \tag{18}$$

and

$$\mathbf{H}^{(1)}_{s\uparrow-\uparrow} = \begin{array}{c} \\ \vdots \\ s-2_\uparrow \\ s-1_\uparrow \\ s_{\uparrow\Downarrow} \\ s_{\downarrow\Uparrow} \\ s{+}1_\uparrow \\ s{+}2_\uparrow \\ \vdots \end{array} \begin{array}{c} \cdots \quad s-2_\uparrow \quad s-1_\uparrow \quad s_{\uparrow\Downarrow} \quad s_{\downarrow\Uparrow} \quad s{+}1_\uparrow \quad s{+}2_\uparrow \quad \cdots \\ \begin{pmatrix} \ddots & \ddots & & & & & & \\ \ddots & \varepsilon_0 & -t & & & & & \\ & -t & \varepsilon_0 & -t' & & & & \\ & & -t' & \frac{-J}{4} & \frac{J}{2} & -t' & & \\ & & & \frac{J}{2} & \frac{-J}{4} & 0 & & \\ & & & -t' & 0 & \varepsilon_0 & -t & \\ & & & & & -t & \varepsilon_0 & \ddots \\ & & & & & & \ddots & \ddots \end{pmatrix} \end{array}. \tag{19}$$

The matrices $\mathbf{H}^{(1)}_{s\uparrow-\downarrow}$ and $\mathbf{H}^{(1)}_{s\uparrow-\uparrow}$ are exactly equal to $\mathbf{H}_A$ and $\mathbf{H}_B$, respectively, by replacing the tight-binding parameters ε_α in Eqs. 12 and 13 with $-J/4$, and $-t''$ in Eqs. 12 and 13 with $J/2$.

Replacing these parameters and recalculating the transmission probabilities using Green's function approach, we obtained the transmission probabilities in ↑-to-↑ and ↑-to-↓ processes, as shown in Fig. 7. In spite of the simple matrix division, the correspondence between the transmission probabilities in the wave-packet propagation and those in Green's function is quite well, except for the transmission at the resonance levels ($-0.15\ t$ and $0.05\ t$) and at the anti-resonance level ($-\ 0.05\ t$) in the ↑-to-↑ transport. Although we cannot obtain a quantitative agreement in transmission probabilities at the resonance/anti-resonance levels, Green's function approach can capture the spin-flip transport properties qualitatively: (1) the peaks appear at the eigenlevel of the singlet and triplet states, (2) the ↑-to-↓ transport shows a moderate decrease at the anti-resonance level, and (iii) the ↑-to-↑ transport shows an abrupt drop at the anti-resonance level. Referring to the orbital concept for the coherent electron transport described in the two-site model, we can conclude that the moderate decrease in ↑-to-↓ transport at the anti-resonance level is the result of a coherent-and-cooperative contribution from the singlet and triplet states of the conduction and localized electron spins, and that, the abrupt drop in ↑-to-↑ transport at the anti-resonance level is mainly caused by the coherent cancellation from the singlet and triplet states.

3.3 Spin-flip transport including *quasi*-incoherent processes in Green's function approach

The discrepancies between the wave-packet propagation and Green's function approach appear only at the resonant/anti-resonant peaks. Since the lifetime at the resonant level is much longer than that at no-resonant level, we can speculate that the incoherent multiple spin-flips occur at these levels. In addition, the approximation made in the previous part includes a clear shortcoming that the division of the whole processes into the ↑-to-↑ and ↑-to-↓ processes eliminates the interference between the two processes. In general, to take the incoherent and interference effects into account in Green's function approach, we can introduce fictitious probes by assuming an *appropriate* self-energy [44].

In the present *s-d* Hamiltonian divided into the ↑-to-↓ and ↑-to-↑ processes, $\mathbf{H}^{(1)}_{s\uparrow-\downarrow}$ and $\mathbf{H}^{(1)}_{s\uparrow-\uparrow}$, the interference between the divided two processes can be included in Green's function by assuming a fictitious interaction t' between the spin sites and fictitious probes. In fact, the matrix division into the ↑-to-↑ and ↑-to-↓ processes was carried out by neglecting the single interaction t', [4] that is, the 2×2 self-energy matrix for the spin sites $\mathbf{\Sigma}^s$ has a single non-zero element as

$$\left(\mathbf{\Sigma}^s_{s\uparrow\Downarrow}\right)_{i,j} = t'^2 g_{\mathrm{elec}} \delta_{ij}\delta_{i1}, \left(\mathbf{\Sigma}^s_{s\downarrow\Uparrow}\right)_{i,j} = t'^2 g_{\mathrm{elec}} \delta_{ij}\delta_{i2} (\text{for} \uparrow \text{to} \downarrow), \tag{20}$$

and

$$\left(\mathbf{\Sigma}^s_{s\uparrow\Downarrow}\right)_{i,j} = t'^2 g_{\mathrm{elec}} \delta_{ij}\delta_{i2}, \left(\mathbf{\Sigma}^s_{s\downarrow\Uparrow}\right)_{i,j} = t'^2 g_{\mathrm{elec}} \delta_{ij}\delta_{i2} (\text{for} \uparrow \text{to} \uparrow). \tag{21}$$

Using the self-energies, each spin site (i.e., $s\uparrow\Downarrow$ or $s\downarrow\Uparrow$) is connected to the two probes in both processes, and thereby,

[4] For the ↑-to-↓ case, we picked up the matrix elements in $\mathbf{H_s}$ relating to the ↑-to-↓ process by neglecting the matrix element $(\mathbf{H}_s)_{s\uparrow,\Downarrow,\, s+1\uparrow} (= -t')$ and for the ↑-to-↑ case by neglecting the matrix element $(\mathbf{H_s})_{s\downarrow,\Uparrow,\, s+1\downarrow} (= -t')$.

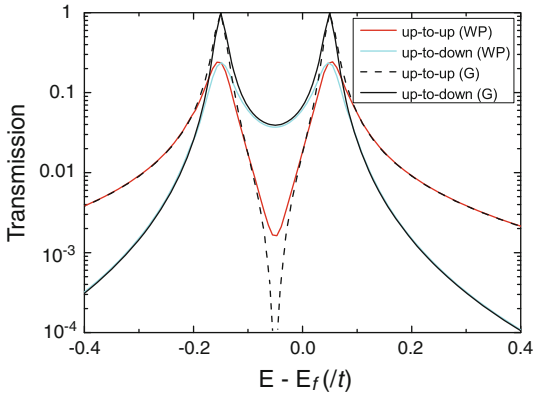

Fig. 7 Calculated transmission probabilities for the ↑-to-↑ and ↑-to-↓ processes in Green's function approach (G) and in wave-packet propagation (WP). The tight-binding parameters adopted in the calculations are the same used in Fig. 3 ($t' = 0.1\ t$, $J = 0.2\ t$)

the system can be regarded as a symmetric four probe system. The Green's function including the four self-energies in total (i.e., the four-terminal Green's function) is

$$\mathbf{G}_4^{A/R}(E) = \left[E\mathbf{1} - \mathbf{H}_{\text{spin}}^{(1)} - \mathbf{\Sigma}_L^{A/R} - \mathbf{\Sigma}_R^{A/R} - \mathbf{\Sigma}_{s\uparrow\Downarrow}^{s,A/R} - \mathbf{\Sigma}_{s\downarrow\Uparrow}^{s,A/R}\right]^{-1}, \tag{22}$$

where $\mathbf{H}_{\text{spin}}^{(1)}$ is the 2×2 matrix for the basis of $s\uparrow\Downarrow$ and $s\downarrow\Uparrow$ in Eqs. 18 and 19.

Figure 8a shows the calculated transmission probability using the four-terminal Green's function; the same tight-binding parameters in Figs. 3 and 7 were again adopted. In both of the ↑-to-↑ and ↑-to-↓ processes, the discrepancies at the resonance levels ($-0.15\ t$ and $0.05\ t$) completely disappear in the four-terminal Green's function calculations. In addition, the zero of the transmission in the two-terminal Green's function at the anti-resonance level ($-\ 0.05\ t$) for the ↑-to-↑ process is also significantly improved to be a small non-zero number, 1.5×10^{-3}, being almost identical to the value from the wave-packet propagation. These improvements clearly indicate that the incoherent or interference effects in the spin-flip processes are effectively included in the four-terminal Green's function through the self-energies from the fictitious probes defined in Eqs. 20 and 21. It is worth mentioning that there are no fitting parameters for the fictitious probes in the present four-terminal Green's function.

In order to confirm the applicability of the four-terminal Green's function for the spin-flip transport, we calculated the transmission probabilities using different tight-binding parameters J and t'. Figure 8b, c show the calculated transmission probabilities using $J = 0.4\ t$ and $J = 0.05\ t$, respectively, together with the hopping parameter $t' = 0.1\ t$, to investigate the J dependence.[5] The correspondences between the four-terminal Green's function approach and wave-packet propagations are excellent, as can be seen in Fig. 8a. In order to check the weak and strong coupling cases for the hopping parameter t' between the molecule and electrodes, we calculated transmission probabilities using (J, t') of ($0.5\ t$, $0.5\ t$) for the strong coupling and ($0.05\ t$, $0.05\ t$) for the weak coupling. Excellent agreements were again obtained in these cases. It is to be noted that the slight difference for the ↑-to-↑ transport at the anti-resonance level in the weak coupling case (Fig. 8e) is merely caused by the lack of the extremely fine energy mesh in the wave-packet propagation.

The transmission probabilities shown in Fig. 8 are the transmission functions for the direct term from the left to right electrodes: $T_{LR}(E) = \text{Tr}\left[i\left\{\mathbf{\Sigma}_L^R(E) - \mathbf{\Sigma}_L^A(E)\right\}\mathbf{G}_4^R(E)\ i\left\{\mathbf{\Sigma}_R^R(E) - \mathbf{\Sigma}_R^A(E)\right\}\mathbf{G}_4^A(E)\right]$. That is, the transmission functions does not include the correction terms [44] representing the transmission from the fictitious probes to the realistic ones and vice versa. However, the transmission functions are the ones reproducing the transmission probabilities from the wave-packet propagations. This means that the present wave-packet propagations do include incoherent spin-flip processes partially, *quasi*-incoherent processes. In other words, the electron exchanges between the realistic system and fictitious electron reservoir, which definitely destroy the coherency, are not included in. This situation is probably comprehensible according to the following observation that there are no ambiguous terms leading to randomized phase-breaking processes in the wave-packet propagations based on the *s-d* Hamiltonian. This observation will in turn inspire us so as to include many-body effects in the spin-flip transport (i.e., Kondo effects) by assigning *realistic* chemical potentials to the fictitious reservoirs and by including the correction terms representing the transmission from the fictitious reservoirs to the realistic systems. The issue will be investigated in the near future.

[5] When the molecule is in an isolated situation, we can use the spin-orbit interaction for the calculations of J. However, the molecular junction in which the spin-flip is caused by the incoming electrons from an electrode is clearly different from an isolated molecule in which an electron leading to the spin-flip is stationary captured by the molecule. That is, even when we adopted the spin-orbit interaction, the applicability of the strategy is still ambiguous for the present target. Thus we adopted the s-d Hamiltonian as the first step in this study because the Hamiltonian is clearly constructed from the conduction *s*-electrons and localized spin on the *d*-level. To investigate the parameter dependence on the spin-flip transport, we simulated the spin-flip dynamics using a strong/weak spin-spin interaction J with a strong/weak electrode-molecule coupling t', as shown in Fig. 8.

4 Summary

We investigated the *spin-flip transport* in a simple one-dimensional tight-binding chain including a localized spin on the basis of the wave-packet dynamics and Green's function approach. The spin exchange coupling J between the conduction and localized electron spins was taken into account through the *s-d* Hamiltonian. The wave-packet propagations were carried out using the Crank-Nicholson scheme, and the spin transmission probabilities for the incoming polarized electron (up-spin) at the source electrode were calculated by assuming the anti-ferromagnetic coupling between the conduction and localized electron spins. From the wave-packet dynamics, we obtained the transmission probabilities depending on the spin directions at the drain electrode: the ↑-to-↑ process for the incoming up-spin transmitted as the outgoing up-spin, and the ↑-to-↓ process for the incoming up-spin transmitted as the outgoing down-spin. We found in the wave-packet simulations that the transmission probabilities in both processes show large peaks at the eigenlevels of the spin singlet ($-3J/4$) and triplet ($J/4$) states, and that, the transmission probabilities show different properties depending on the spin-flip processes at the mid-gap (anti-resonance level) of the two eigenlevels: the ↑-to-↑ process shows an abrupt drop, but the ↑-to-↓ process a moderate drop at the energy. Referring to the orbital concept for the coherent electron transport in a molecular junction on the basis of the two-terminal Green's function approach, we can qualitatively understand that the moderate decrease in ↑-to-↓ transport at the anti-resonance level is the result of a coherent-and-cooperative contribution from the singlet and triplet states of the conduction and localized electron spins, and that, the abrupt drop in ↑-to-↑ transport at the anti-resonance level is mainly caused by the coherent cancellation from the singlet and triplet states.

To achieve more quantitative understandings for the spin-flip dynamics, we introduced a four-terminal Green's function, in which two fictitious probes were introduced to represent the incoherent and/or interference effects between the ↑-to-↑ and ↑-to-↓ processes. We defined the self-energies for the fictitious probes without ambiguity, and successfully obtained excellent correspondences in transmission probabilities between the four-terminal Green's function approach and wave-packet dynamics, regardless of the tight-binding parameters. Since the transmission functions calculated in the four-terminal Green's function approach include the incoherent spin-flip processes partially, we can conclude that the present wave-packet propagations correspond to *quasi*-incoherent spin-flip simulations. We finally proposed that a standard treatment of the fictitious probes by assigning realistic chemical potentials to those in the four-terminal Green's functions has a possibility to be a simple theoretical tool for the spin-dependent electron transport, including many-body effects. We believe that our findings on the spin-flip transport will be the basic for the understanding of the spin-dependent transport in molecular spin junctions, and that, it serves the basic model for the molecular spin design in single molecular junctions.

Acknowledgments It is a great pleasure to dedicate this paper to Prof. A. Imamura, who was a supervisor of one of the authors (TT) in Hiroshima University from 1995 to 1998. The lectures on the molecular orbital theory given by A. Imamura have continued to inspire the interests of one of the authors (TT) in the field of the molecular science. This work was partially supported by the Grant-in-Aid for Young Scientists (B), MEXT of Japan. The author would like to thank S. Konabe for technical information on wave-packet dynamics.

Appendix 1: *s-d* Hamiltonian

The one-dimensional system adopted in this study is composed of electrodes and a localized electron spin. This system, thus, can be regarded as a metal including a single impurity spin. The Anderson Hamiltonian is an appropriate model to investigate the magnetic property of the metal with impurities, and we use the Anderson Hamiltonian to derive the *s-d* Hamiltonian, which is the story introduced in the book by Shiba [53]. The Anderson Hamiltonian is written as

$$H = \sum_{k\sigma} \varepsilon_k c_{k\sigma}^{\dagger} c_{k\sigma} + \sum_{\sigma} \varepsilon_d n_{d\sigma} + U n_{d\uparrow} n_{d\downarrow} + \frac{1}{\sqrt{N_A}} \sum_{k\sigma} \left(V_k c_{k\sigma}^{\dagger} d_{\sigma} + \text{h.c.} \right). \quad (23)$$

The first term represents the Hamiltonian of conduction electrons in electrodes, and ε_d in the second term is the impurity d-level. The on-site energy U in the third term represents the coulomb interaction when the impurity d-level is occupied by two electrons. The forth term is the interaction between the orbitals in electrodes and the impurity. $c_{\sigma}^{\dagger}$ and $d_{\sigma}^{\dagger}$ (c_{σ} and d_{σ}) are the creation (annihilation) operators of an electron with spin σ in the electrodes and impurity level, respectively; $n_{d\sigma}$ is the number operator, $d_{\sigma}^{\dagger} d_{\sigma}$, and N_A is the total number of atoms. To investigate physical properties of the system described with the Anderson Hamiltonian, there are two standard approaches: (1) the third term in Eq. 23 is considered as a perturbation, and (2) the fourth term in Eq. 23 is considered as a perturbation. The latter approach is more suitable for the present one-dimensional model including a single localized spin, that is, the unperturbed Hamiltonian H_0 and perturbation term H_I are

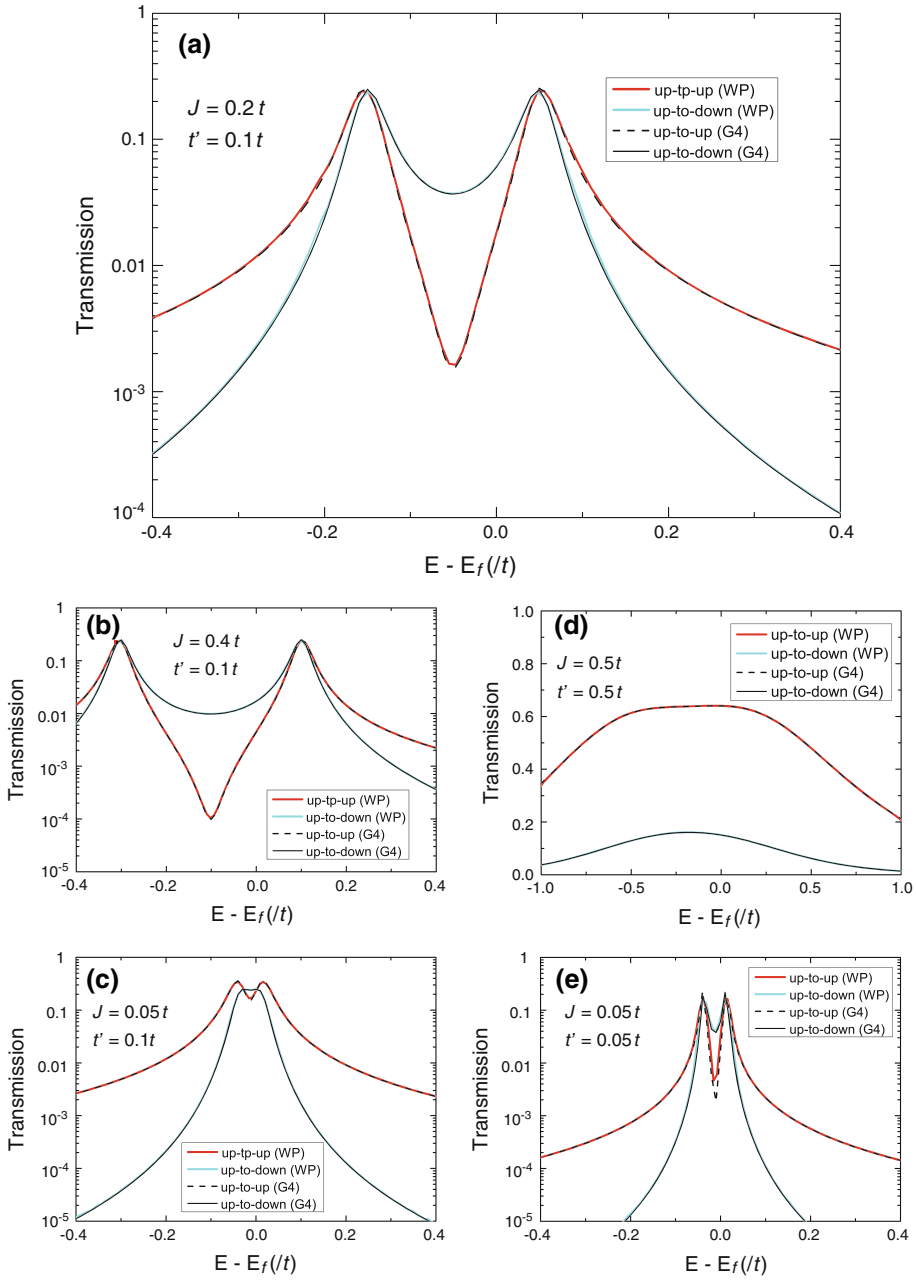

Fig. 8 Calculated transmission probabilities for the ↑-to-↑ and ↑-to-↓ processes in the four-terminal Green's function approach (G4) and in wave-packet propagation (WP). The tight-binding parameters adopted in these calculations are **a** $J = 0.2\ t$, $t' = 0.1\ t$, **b** $J = 0.4\ t$, $t' = 0.1\ t$, **c** $J = 0.05\ t$, $t' = 0.1\ t$, **d** $J = 0.5\ t$, $t' = 0.5\ t$, and **e** $J = 0.05\ t$, $t' = 0.05\ t$

$$H_0 = \sum_{k\sigma} \varepsilon_k c^{\dagger}_{k\sigma} c_{k\sigma} + \sum_{\sigma} \varepsilon_d n_{d\sigma} + U n_{d\uparrow} n_{d\downarrow}, \tag{24}$$

and

$$H_I = \frac{1}{\sqrt{N_A}} \sum_{k\sigma} \left(V_k c^{\dagger}_{k\sigma} d_{\sigma} + \text{h.c.} \right), \tag{25}$$

respectively. The unperturbed Green's function $G_0(E)$ and perturbed Green's function $G(E)$ can be represented as $(E - H_0)^{-1}$ and $(E - H)^{-1}$, respectively. Using the relation $(A - B)^{-1} = A^{-1} + A^{-1}BA^{-1} + A^{-1}BA^{-1}BA^{-1} + \cdots$, we straightforwardly obtain the perturbed Green's function in terms of G_0 and H_I as

$$\begin{aligned} G = {} & G_0 + G_0 H_I G_0 + G_0 H_I G_0 H_I G_0 \\ & + G_0 H_I G_0 H_I G_0 H_I G_0 + \cdots . \end{aligned} \tag{26}$$

This is useful to define the effective Hamiltonian of the perturbation term.

Let us firstly consider the system in which the d-level is occupied by an electron and investigate the effects from the interactions between the d-level and conduction levels. The

unperturbed states are represented as $d_\uparrow^\dagger|F\rangle$ and $d_\downarrow^\dagger|F\rangle$, where $|F\rangle$ indicates conduction electrons occupying the levels ε_k up to the Fermi level. When we consider the first-order process H_I (i.e., $V_k c_{k\sigma}^\dagger d_\sigma$) with respect to the unperturbed states $d_\uparrow^\dagger|F\rangle$ and $d_\downarrow^\dagger|F\rangle$, we can easily find that the expectation values of the first-order process are vanished because of the following relations: $d_\sigma|F\rangle = 0$ and $\langle F|d_\sigma^\dagger = 0$. For example, the first-order term for $d_\uparrow^\dagger|F\rangle$ has the form of $\langle F|d_\uparrow c_{k\sigma}^\dagger d_\sigma d_\uparrow^\dagger|F\rangle$ or $\langle F|d_\uparrow d_\sigma^\dagger c_{k\sigma} d_\uparrow^\dagger|F\rangle$. The observation allows us to rewrite the perturbed Green's function as

$$G = G_0 + G_0 H_I G_0 H_I G_0 + G_0 H_I G_0 H_I G_0 H_I G_0 H_I G_0 + \cdots. \tag{27}$$

Defining the second-order term $H_I\, G_0\, H_I$ as H_I^{eff}, we obtain

$$G = G_0 + G_0 H_I^{\mathrm{eff}} G_0 + G_0 H_I^{\mathrm{eff}} G_0 H_I^{\mathrm{eff}} G_0 + \cdots. \tag{28}$$

This is the perturbed Green's function for the Hamiltonian of $H_0 + H_I^{\mathrm{eff}}$. Thus, we consider the second-order processes $H_I\, G_0\, H_I$ to obtain the explicit form of the effective Hamiltonian. It is to be noted that the unperturbed Green's function G_0 is a function of energy E, and the energy dependence in the effective Hamiltonian $H_I\, G_0\, H_I$ is not convenient for general use. However, the perturbed states in which the energy is close to the unperturbed energy $E_0 (= \sum_{k'}^{\mathrm{occ}} \varepsilon_{k'} + \varepsilon_d)$ are well mixed with the unperturbed state, and the effective Hamiltonian derived from $H_I\, G_0(E_0)\, H_I$ can be recognized as a reasonable one.

Let us next consider the explicit form of the second-order process. There are two types for the intermediate states in which zero/two electrons occupy the d-level. For the zero occupation case with the initial state of $d_\uparrow^\dagger|F\rangle$, we have

$$\frac{1}{E_0 - H_0} V c_{k\uparrow}^\dagger d_\uparrow d_\uparrow^\dagger |F\rangle = \frac{1}{\varepsilon_d - \varepsilon_k} V c_{k\uparrow}^\dagger |F\rangle, \tag{29}$$

where we use the anticommutator relation of Fermions (e.g., $[c_k, c_{k'}^\dagger]_+ = \delta_{k,k'}$) and the fact $H_0 c_{k\uparrow}^\dagger d_\uparrow d_\uparrow^\dagger |F\rangle = (\sum_{k'}^{\mathrm{occ}} \varepsilon_{k'} + \varepsilon_k) c_{k\uparrow}^\dagger d_\uparrow d_\uparrow^\dagger |F\rangle$. Operating H_I at the left-hand side of Eq. 29, we obtain

$$\begin{aligned} & V\left(d_\uparrow^\dagger c_{k''\uparrow} + d_\downarrow^\dagger c_{k''\downarrow}\right) \frac{1}{\varepsilon_d - \varepsilon_k} V c_{k\uparrow}^\dagger |F\rangle \\ &= \frac{V^2}{\varepsilon_d - \varepsilon_k}\left(d_\uparrow^\dagger c_{k''\uparrow} c_{k\uparrow}^\dagger + d_\downarrow^\dagger c_{k''\downarrow} c_{k\uparrow}^\dagger\right)|F\rangle \\ &= \frac{V^2}{\varepsilon_d - \varepsilon_k}\left(\delta_{k,k''} d_\uparrow^\dagger - c_{k\uparrow}^\dagger c_{k''\uparrow} d_\uparrow^\dagger - c_{k\uparrow}^\dagger c_{k''\downarrow} d_\downarrow^\dagger\right)|F\rangle. \end{aligned} \tag{30}$$

Since the expectation value of the process is obtained by applying $\langle F|d_\sigma$ at the left-hand side of Eq. 30, we readily confirm the second-order processes have non-zero expectation values.

For the initial state of $d_\downarrow^\dagger|F\rangle$ in the zero occupation case, we have

$$\frac{1}{E_0 - H_0} V c_{k\downarrow}^\dagger d_\downarrow d_\downarrow^\dagger |F\rangle = \frac{1}{\varepsilon_d - \varepsilon_k} V c_{k\downarrow}^\dagger |F\rangle, \tag{31}$$

and obtain the following expression by operating H_I at the left-hand side of Eq. 31 as

$$\begin{aligned} & V\left(d_\uparrow^\dagger c_{k''\uparrow} + d_\downarrow^\dagger c_{k''\downarrow}\right) \frac{1}{\varepsilon_d - \varepsilon_k} V c_{k\downarrow}^\dagger |F\rangle \\ &= \frac{V^2}{\varepsilon_d - \varepsilon_k}\left(d_\uparrow^\dagger c_{k''\uparrow} c_{k\downarrow}^\dagger + d_\downarrow^\dagger c_{k''\downarrow} c_{k\downarrow}^\dagger\right)|F\rangle \\ &= \frac{V^2}{\varepsilon_d - \varepsilon_k}\left(\delta_{k,k''} d_\downarrow^\dagger - c_{k\downarrow}^\dagger c_{k''\uparrow} d_\uparrow^\dagger - c_{k\downarrow}^\dagger c_{k''\downarrow} d_\downarrow^\dagger\right)|F\rangle. \end{aligned} \tag{31}$$

For the doubly occupation case with the initial states of $d_\uparrow^\dagger|F\rangle$ and $d_\downarrow^\dagger|F\rangle$, we, respectively, have

$$\begin{aligned} & V\left(c_{k'\uparrow}^\dagger d_\uparrow + c_{k'\downarrow}^\dagger d_\downarrow\right) \frac{1}{\varepsilon_k - \varepsilon_d - U} V d_\downarrow^\dagger c_{k\downarrow} d_\uparrow^\dagger |F\rangle \\ &= \frac{V^2}{\varepsilon_k - \varepsilon_d - U}\left(-c_{k'\uparrow}^\dagger c_{k\downarrow} d_\downarrow^\dagger + c_{k'\downarrow}^\dagger c_{k\downarrow} d_\uparrow^\dagger\right)|F\rangle, \end{aligned} \tag{33}$$

and

$$\begin{aligned} & V\left(c_{k''\uparrow}^\dagger d_\uparrow + c_{k''\downarrow}^\dagger d_\downarrow\right) \frac{1}{\varepsilon_k - \varepsilon_d - U} V d_\uparrow^\dagger c_{k\uparrow} d_\downarrow^\dagger |F\rangle \\ &= \frac{V^2}{\varepsilon_k - \varepsilon_d - U}\left(-c_{k''\downarrow}^\dagger c_{k\uparrow} d_\uparrow^\dagger + c_{k''\uparrow}^\dagger c_{k\uparrow} d_\downarrow^\dagger\right)|F\rangle. \end{aligned} \tag{34}$$

From Eqs. 30, 32–34, we obtain the expression of the effective Hamiltonian with respect to $|F\rangle$ as

$$\begin{aligned} & \frac{V^2}{\varepsilon_d - \varepsilon_k}\left(\delta_{k,k''} d_\uparrow^\dagger - c_{k\uparrow}^\dagger c_{k''\uparrow} d_\uparrow^\dagger - c_{k\uparrow}^\dagger c_{k''\downarrow} d_\downarrow^\dagger \right. \\ & \left. + \delta_{k,k''} d_\downarrow^\dagger - c_{k\downarrow}^\dagger c_{k''\downarrow} d_\downarrow^\dagger - c_{k\downarrow}^\dagger c_{k''\uparrow} d_\uparrow^\dagger\right) \\ & + \frac{V^2}{\varepsilon_k - \varepsilon_d - U}\left(-c_{k''\uparrow}^\dagger c_{k\downarrow} d_\downarrow^\dagger + c_{k''\downarrow}^\dagger c_{k\downarrow} d_\uparrow^\dagger \right. \\ & \left. - c_{k''\downarrow}^\dagger c_{k\uparrow} d_\uparrow^\dagger + c_{k''\uparrow}^\dagger c_{k\uparrow} d_\downarrow^\dagger\right). \end{aligned} \tag{35}$$

Since this Hamiltonian is derived using the singly occupied d-level (i.e., $d_\uparrow^\dagger|F\rangle$ and $d_\downarrow^\dagger|F\rangle$), the creation operators for the d-level must be replaced with the number operators for general use. The effective Hamiltonian, thus, can be represented as

$$H_I^{\text{eff}} = \frac{1}{N_A}\sum_{k,k''}\Big[\frac{V^2}{\varepsilon_d-\varepsilon_k}\Big(-c_{k\uparrow}^\dagger c_{k''\uparrow}d_\uparrow^\dagger d_\uparrow - c_{k\uparrow}^\dagger c_{k''\downarrow}d_\downarrow^\dagger d_\uparrow - c_{k\downarrow}^\dagger c_{k''\downarrow}d_\downarrow^\dagger d_\downarrow - c_{k\downarrow}^\dagger c_{k''\uparrow}d_\uparrow^\dagger d_\downarrow\Big) + \frac{V^2}{\varepsilon_k-\varepsilon_d-U}\Big(-c_{k''\uparrow}^\dagger c_{k\downarrow}d_\downarrow^\dagger d_\uparrow + c_{k''\downarrow}^\dagger c_{k\downarrow}d_\uparrow^\dagger d_\uparrow - c_{k''\downarrow}^\dagger c_{k\uparrow}d_\uparrow^\dagger d_\downarrow + c_{k''\uparrow}^\dagger c_{k\uparrow}d_\downarrow^\dagger d_\downarrow\Big)\Big], \tag{36}$$

where we omitted several terms that do not include the operators of conduction electrons for simplicity. Using the relations for the number counting and spin-flip operators, $n_{d\sigma} = d_\sigma^\dagger d_\sigma, S_+ = d_\uparrow^\dagger d_\downarrow$, and $S_- = d_\downarrow^\dagger d_\uparrow$, we have

$$H_I^{\text{eff}} = \frac{1}{N_A}\sum_{k,k''}\Big[\frac{V^2}{\varepsilon_d-\varepsilon_k}\Big(-c_{k\uparrow}^\dagger c_{k''\uparrow}n_{d\uparrow} - c_{k\uparrow}^\dagger c_{k''\downarrow}S_- - c_{k\downarrow}^\dagger c_{k''\downarrow}n_{d\downarrow} - c_{k\downarrow}^\dagger c_{k''\uparrow}S_+\Big) + \frac{V^2}{\varepsilon_k-\varepsilon_d-U}\Big(-c_{k''\uparrow}^\dagger c_{k\downarrow}S_- + c_{k''\downarrow}^\dagger c_{k\downarrow}n_{d\uparrow} - c_{k''\downarrow}^\dagger c_{k\uparrow}S_+ + c_{k''\uparrow}^\dagger c_{k\uparrow}n_{d\downarrow}\Big)\Big]. \tag{37}$$

Since the energy difference between ε_k and the Fermi level is smaller than ε_d and $\varepsilon_d + U$, the effective Hamiltonian can be written as

$$H_I^{\text{eff}} = \frac{1}{N_A}\sum_{k,k''}\Big[V^2\Big(-\frac{1}{\varepsilon_d}-\frac{1}{\varepsilon_d+U}\Big)\times\Big(c_{k\uparrow}^\dagger c_{k''\uparrow}+c_{k\downarrow}^\dagger c_{k''\downarrow}\Big)\times\big(n_{d\uparrow}+n_{d\downarrow}\big) + V^2\Big(-\frac{1}{\varepsilon_d}+\frac{1}{\varepsilon_d+U}\Big)\Big(c_{k\uparrow}^\dagger c_{k''\downarrow}S_- + c_{k\downarrow}^\dagger c_{k''\uparrow}S_+\Big)\Big]. \tag{38}$$

Using the condition $n_{d\uparrow} + n_{d\downarrow} = 1$, we reasonably obtain the effective Hamiltonian as

$$H_I^{\text{eff}} = \frac{1}{N_A}\sum_{k,k',\sigma}\frac{V^2}{2}\Big(-\frac{1}{\varepsilon_d}-\frac{1}{\varepsilon_d+U}\Big)c_{k\sigma}^\dagger c_{k'\sigma} + \frac{1}{N_A}\sum_{k,k',\sigma,\sigma'}V^2\Big(-\frac{1}{\varepsilon_d}+\frac{1}{\varepsilon_d+U}\Big)c_{k\sigma}^\dagger\,\sigma_{\sigma,\sigma'}c_{k'\sigma'}\cdot\mathbf{S}, \tag{39}$$

where $\boldsymbol{\sigma}$ is the Pauli matrix,

$$\boldsymbol{\sigma}_{\mathbf{x}} = \begin{array}{c}\\ \uparrow\\ \downarrow\end{array}\!\!\begin{array}{c}\begin{array}{cc}\uparrow & \downarrow\end{array}\\ \begin{pmatrix}0 & 1\\ 1 & 0\end{pmatrix}\end{array}, \boldsymbol{\sigma}_{\mathrm{y}} = \begin{array}{c}\\ \uparrow\\ \downarrow\end{array}\!\!\begin{array}{c}\begin{array}{cc}\uparrow & \downarrow\end{array}\\ \begin{pmatrix}0 & -i\\ i & 0\end{pmatrix}\end{array}, \boldsymbol{\sigma}_{\mathbf{z}} = \begin{array}{c}\\ \uparrow\\ \downarrow\end{array}\!\!\begin{array}{c}\begin{array}{cc}\uparrow & \downarrow\end{array}\\ \begin{pmatrix}1 & 0\\ 0 & -1\end{pmatrix}\end{array}, \tag{40}$$

and we use the following relations, $S_+ = S_x + i\ S_y$ and $S_- = S_x - i\ S_y$. The first term represents the potential scattering process that are independent of the spin-direction. The second term represents the spin-dependent scattering processes including spin-flip processes. Regarding the term $-2V^2\left(-\frac{1}{\varepsilon_d}+\frac{1}{\varepsilon_d+U}\right)$ as the spin-spin interaction J, we finally obtain the *s-d* Hamiltonian as

$$H_{s-d} = -\frac{J}{2N_A}\sum_{k,k'',\sigma,\sigma'}c_{k\sigma}^\dagger\boldsymbol{\sigma}_{\sigma,\sigma'}c_{k''\sigma'}\cdot\mathbf{S}. \tag{41}$$

From the *s-d* Hamiltonian, we easily obtain the matrix elements in the spin sub-space as follows:

$$\mathbf{H_{sd}} = \begin{array}{c}\\ \uparrow\Uparrow\\ \downarrow\Downarrow\\ \uparrow\Downarrow\\ \downarrow\Uparrow\end{array}\!\!\begin{array}{c}\begin{array}{cccc}\uparrow\Uparrow & \downarrow\Downarrow & \uparrow\Downarrow & \downarrow\Uparrow\end{array}\\ \begin{pmatrix}\frac{J}{4} & 0 & 0 & 0\\ 0 & \frac{J}{4} & 0 & 0\\ 0 & 0 & -\frac{J}{4} & \frac{J}{2}\\ 0 & 0 & \frac{J}{2} & -\frac{J}{4}\end{pmatrix}\end{array}. \tag{42}$$

It is to be noted that the factor N_A is taken into account through the normalized amplitudes in the wave packets.

Appendix 2: The Crank-Nicholson scheme

The time-dependent Schrödinger equation is

$$i\frac{\partial\psi}{\partial t} = H\psi, \tag{43}$$

and the formal solution of the equation is

$$\psi(x,t) = e^{-iHt}\psi(x,0). \tag{44}$$

When we introduce the finite grid for time with the interval of Δt, the wave function after the time propagation of Δt can be written as

$$\psi(x,t+\Delta t) = (1 - iH\Delta t)\psi(x,t). \tag{45}$$

This is accurate up to the first order in time. However, it is well known that the strategy in Eq. 45 is numerically unstable and the time propagation operator is not unitary. To avoid these difficulties, we consider the time propagation in the reverse direction, $t + \Delta t \rightarrow t$. In this case, we have the following relation:

$$\psi(x,t) = (1 + iH\Delta t)\psi(x,t+\Delta t). \tag{46}$$

Using Eqs. 45 and 46, the wave function at $t + \Delta t/2$ is written as

$$\psi(x,t+\Delta t/2) = (1 - iH\Delta t/2)\psi(x,t) \tag{47}$$

and

$$\psi(x,t+\Delta t/2) = (1 + iH\Delta t/2)\psi(x,t+\Delta t). \tag{48}$$

Eliminating the term $\psi(x,t+\Delta t/2)$ using Eqs. 47 and 48, we obtain

$$(1 + iH\Delta t/2)\psi(x, t + \Delta t) = (1 - iH\Delta t/2)\psi(x, t), \quad (49)$$

and thereby

$$\psi(x, t + \Delta t) = \frac{(1 - iH\Delta t/2)}{(1 + iH\Delta t/2)}\psi(x, t). \quad (50)$$

We can easily confirm that the time propagation operator $\frac{(1-iH\Delta t/2)}{(1+iH\Delta t/2)}$ is unitary and that the time propagation is accurate up to the second order in time using the standard mathematical relations: $e^A = 1 + A + \frac{1}{2!}A^2 + \cdots$ and $(1 + A)^{-1} = 1 - A + A^2 - A^3 \cdots$.

Appendix 3: The computational conditions for wave-packet simulations

There are two important computational conditions for wave-packet simulations: (1) the energy resolution in the wave-packet simulation must be quite fine in order to compare the results with those from Green's function method and (2) we have to take care that an artificial reflection of the wave-packet at the left-/right-hand edge of the one-dimensional chain does not affect the true dynamics of the wave-packet scattered by the localized spin. As for the first point, the Gaussian type of wave-packet is adopted in this study, and thereby, the wave-packet is spatially well broadened when the energy of the wave-packet is finely focused on a certain value. This is very important for the calculations of the transmission functions from wave-packet dynamics as a function of energy. We tested several Gaussian wave-packets having different broadening width and consequently found that the wave-packet with broadening width of 1,200 sites or more is sufficient for the calculations of transmission functions and for the comparison with Green's function results. As for the second point, we have to recognize that the firstly reflected wave-packet at the central spin site will arrive at the left-hand edge of the one-dimensional chain and in turn propagates again toward the spin site. If a portion of the wave-packet is trapped on the spin site (this will be probable for the weak interaction between the electrode and molecule), an artificial superposition between the trapped wave-packet and re-reflected wave-packet occurs. Since we calculate the transmission probabilities from the transmitted wave-packet at the right electrodes, the artificial superposition will cause the artificial errors in transmission functions. We of course take care about the reflection of the transmitted wave-packet at the right-hand edge, too. To avoid the artificial errors caused by the re-reflected wave-packets at the left-/right-hand edge, we simply adopted a large number of sites, 20,000 in this study, and confirmed the model size is sufficient for the present purpose.

As for the unit of simulation time, we determined the unit as follows: (1) we first assumed that each site in electrodes corresponds to a carbon atom, and second that the transfer integral t of 1 corresponds to 2.7 eV, which is a typical value in the carbon 2 p_π network; (2) we calculated the Fermi velocity from the energy band dispersion in the one-dimensional carbon chain, using the carbon–carbon bond distance of 1.4 Å; and (3) we determined the velocity of the right-moving wave packet at the Fermi level (i.e., the unit of simulation time) so as to be identical to the Fermi velocity calculated in Step 2.

References

1. Kane BE (1998) A silicon-based nuclear spin quantum computer. Nature 393:133
2. Vandersypen LMK, Steffen M, Breyta G, Yannoni CS, Sherwood MH, Chuang IL (2001) Experimental realization of Shor's quantum factoring algorithm using nuclear magnetic resonance. Nature 414:883
3. Jelezko F, Gaebel T, Popa I, Gruber A, Wrachtrup J (2004) Observation of coherent oscillations in a single electron spin. Phys Rev Lett 92:076401
4. Xiao M, Martin I, Yablonovitch E, Jiang HW (2004) Electrical detection of the spin resonance of a single electron in a silicon field-effect transistor. Nature 430:435
5. Childress L, Dutt MVG, Taylor JM, Zibrov AS, Jelezko F, Wrachtrup J, Hemmer PR, Lukin MD (2006) Coherent dynamics of coupled electron and nuclear spin qubits in diamond. Science 314:281
6. Hanson R, Mendoza FM, Epstein RJ, Awschalom DD (2006) Polarization and readout of coupled single spins in diamond. Phys Rev Lett 97:087601
7. McCamey DR, Huebl H, Brandt MS, Hutchison WD, McCallum JC, Clark RG, Hamilton AR (2006) Electrically detected magnetic resonance in ion-implanted Si : P nanostructures. Appl Phys Lett 89:182115
8. Morton JJL, Tyryshkin AM, Brown RM, Shankar S, Lovett BW, Ardavan A, Schenkel T, Haller EE, Ager JW, Lyon SA (2008) Solid-state quantum memory using the 31P nuclear spin. Nature 455:1085
9. Schlegel C, van Slageren J, Manoli M, Brechin EK, Dressel M (2008) Direct observation of quantum coherence in single-molecule magnets. Phys Rev Lett 101:147203
10. Tada T (2008) Hyperfine switching triggered by resonant tunneling for the detection of a single nuclear spin qubit. Phys Lett A 372:6690
11. Smeltzer B, McIntyre J, Childress L (2009) Robust control of individual nuclear spins in diamond. Phys Rev A 80:050302
12. Loth S, von Bergmann K, Ternes M, Otte AF, Lutz CP, Heinrich AJ (2010) Controlling the state of quantum spins with electric currents. Nat Phys 6:340
13. Wang X, Bayat A, Schirmer SG, Bose S (2010) Robust entanglement in antiferromagnetic Heisenberg chains by single-spin optimal control. Phys Rev A 81:032312
14. Park J, Pasupathy AN, Goldsmith JI, Chang C, Yaish Y, Petta JR, Rinkoski M, Sethna JP, Abruña HD, McEuen PL, Ralph DC (2002) Coulomb blockade and the Kondo effect in single-atom transistors. Nature 417:722
15. Liang W, Shores MP, Bockrath M, Long JR, Park H (2002) Kondo resonance in a single-molecule transistor. Nature 417:725
16. Heinrich AJ, Gupta JA, Lutz CP, Eigler DM (2004) Single-atom spin-flip spectroscopy. Science 306:466

17. Wahl P, Diekhöner L, Wittich G, Vitali L, Schneider MA, Kern K (2005) Kondo effect of molecular complexes at surfaces: ligand control of the local spin coupling. Phys Rev Lett 95:166601
18. Zhao A, Li Q, Chen L, Xiang H, Wang W, Pan S, Wang B, Xiao X, Yang J, Hou JG, Zhu Q (2005) Controlling the kondo effect of an adsorbed magnetic ion through its chemical bonding. Science 309:1542
19. Iancu V, Deshpande A, Hla S-W (2006) Manipulating kondo temperature via single molecule switching. Nano Lett 6:820
20. Parks JJ, Champagne AR, Hutchison GR, Flores-Torres S, Abruña HD, Ralph DC (2007) Tuning the kondo effect with a mechanically controllable break junction. Phys Rev Lett 99:026601
21. Gao L, Ji W, Hu YB, Cheng ZH, Deng ZT, Liu Q, Jiang N, Lin X, Guo W, Du SX, Hofer WA, Xie XC, Gao H-J (2007) Site-specific kondo effect at ambient temperatures in Iron-based molecules. Phys Rev Lett 99:106402
22. Chen X, Fu Y-S, Ji S-H, Zhang T, Cheng P, Ma X-C, Zou X-L, Duan W-H, Jia J-F, Xue Q-K (2008) Probing superexchange interaction in molecular magnets by spin-flip spectroscopy and microscopy. Phys Rev Lett 101:197208
23. Sugawara T, Minamoto M, Matsushita MM, Nickels P, Komiyama S (2008) Cotunneling current affected by spin-polarized wire molecules in networked gold nanoparticles. Phys Rev B 77:235316
24. Tsukahara N, Noto K, Ohara M, Shiraki S, Takagi N, Takata Y, Miyawaki J, Taguchi M, Chainani A, Shin S, Kawai M (2009) Adsorption-induced switching of magnetic anisotropy in a single Iron(II) phthalocyanine molecule on an oxidized Cu(110) surface. Phys Rev Lett 102:167203
25. Xue Y, Ratner MA (2003) Microscopic study of electrical transport through individual molecules with metallic contacts. II. Effect of the interface structure. Phys Rev B 68:115407
26. Stokbro K, Taylor J, Brandbyge M, MozosJ-L Ordejón P (2003) Theoretical study of the nonlinear conductance of Di-thiol benzene coupled to Au(111) surfaces via thiol and thiolate bonds. Comput Mater Sci 27:151
27. Nara J, Kino H, Kobayashi N, Tsukada M, Ohno T (2003) Theoretical investigation of contact effects in conductance of single organic molecule. Thin Solid Films 438(439):221
28. Hu Y, Zhu Y, Gao H, Guo H (2005) Conductance of an ensemble of molecular wires: a statistical analysis. Phys Rev Lett 95:156803
29. Ke S-H, Baranger HU, Yang W (2005) Contact atomic structure and electron transport through molecules. J Chem Phys 122:074704
30. Tanibayashi S, Tada T, Watanabe S, Sekino H (2006) Effects of energetic stability in transport measurements of single benzenedithiolate by the STM break junction technique. Chem Phys Lett 428:367
31. Andrews DQ, Van Duyne RP, Ratner MA (2008) Stochastic modulation in molecular electronic transport junctions: molecular dynamics coupled with charge transport calculations. Nano Lett 8:1120
32. Tawara A, Tada T, Watanabe S (2009) Electrostatic and dynamical effects of an aqueous solution on the zero-bias conductance of a single molecule: a first-principles study. Phys Rev B 80:073409
33. Monturet S, Lorente N (2008) Inelastic effects in electron transport studied with wave-packet propagation. Phys Rev B 78:035445
34. Ishii H, Kobayashi N, Hirose K (2010) Order-N electron transport calculations from ballistic to diffusive regimes by a time-dependent wave-packet diffusion method: application to transport properties of carbon nanotubes. Phys Rev B 82:085435
35. Troisi A, Orlandi G (2006) Charge-transport regime of crystalline organic semiconductors: diffusion limited by thermal off-diagonal electronic disorder. Phys Rev Lett 96:086601
36. Kondo N, Yamamoto T, Watanabe K (2006) Phonon wavepacket scattering dynamics in defective carbon nanotubes. Jpn J Appl Phys 45:L963
37. Yao Y, Zhao H, Moore JE, Wu C-Q (2008) Controllable spin-current blockade in a Hubbard chain. Phys Rev B 78:193105
38. Bruus H, Flensberg K (2004) Many-body quantum theory in condensed matter physics, chapter 10. Oxford University Press, Oxford
39. Tada T, Yoshizawa K (2002) Quantum transport effects in nanosized graphite sheets. ChemPhysChem 3:1035
40. Kondo J (1964) Resistance minimum in dilute magnetic alloys. Prog Theor Phys 32:37
41. Press WH, Teukolsky SA, Vetterling WT, Flannery BP (1992) Numerical recipes in fortran 77, 2nd edn. Cambridge University Press, Cambridge
42. Schiff LI (1968) Quantum mechanics, 3rd edn. McGraw-Hill, New York, pp 62–64
43. Caroli C, Combescot R, Nozieres P, Saint-James D (1971) Direct calculation of the tunneling current. J Phys C 4:916
44. Datta S (1995) Electronic transport in mesoscopic systems, chapters 2 and 3. Cambridge University Press, Cambridge
45. Tada T, Yoshizawa K (2003) Quantum transport effects in nanosized graphite sheets. II. Enhanced quantum transport effects by Heteroatoms. J Phys Chem B 107:8789
46. Tada T, Kondo M, Yoshizawa K (2003) Theoretical measurements of conductance in an $(AT)_{12}$ DNA molecule. ChemPhysChem 4:1256
47. Tada T, Yoshizawa K (2004) Reverse exponential decay of electrical transmission in nanosized graphite sheets. J Phys Chem B 108:7565
48. Kondo M, Tada T, Yoshizawa K (2004) Wire-length dependence of the conductance of oligo(p-phenylene) dithiolate wires: a consideration from molecular orbitals. J Phys Chem A 108:9143
49. Tada T, Nozaki D, Kondo M, Hamayama S, Yoshizawa K (2004) Oscillation of conductance in molecular junctions of carbon ladder compounds. J Am Chem Soc 126:14182
50. Tada T, Hamayama S, Kondo M, Yoshizawa K (2005) Quantum transport effects in copper(II) phthalocyanine sandwiched between gold nanoelectrodes. J Phys Chem B 109:12443
51. Kondo M, Tada T, Yoshizawa K (2005) A theoretical measurement of the quantum transport through an optical molecular switch. Chem Phys Lett 412:55
52. Yoshizawa K, Tada T, Staykov A (2008) Orbital views of the electron transport in molecular devices. J Am Chem Soc 130:9406
53. Shiba H (1996) Kotai no denshiron, chapter 4. Maruzen, Tokyo